



## Technical Note

## Practical application of an improved methodology for the double torsion load relaxation method

M. Ciccotti\*, N. Negri, G. Gonzato, F. Mulargia

*Dipartimento di Fisica, Settore di Geofisica, Università di Bologna, Viale Bertini 8 40127, Bologna, Italy*

Accepted 8 April 2001

### 1. Introduction

For most materials the dynamics of subcritical crack propagation during stress-corrosion can be described uniquely by a relationship between the mode-*I* stress intensity factor  $K_I$  and the crack velocity  $v$  that generally has the form of a power law [1]

$$v = AK_I^n \quad (1)$$

with parameters  $A$  and  $n$  (the latter called the stress-corrosion index) depending on the materials properties and on the environmental conditions.

In the last 30 years, the double-torsion load relaxation method (see Fig. 1) has been the most reliable technique for measuring subcritical crack growth, although a considerable scatter in the measured parameters is observed even in the same laboratory [3, 4].

We have recently shown [5, 6] that some of these discrepancies can be traced to the analytical formulation, which provides an incomplete description of the effective deformation of the specimen and of the influence of some important details such as the shape and depth of the side groove and of the initial notch, the curved shape of the crack front profile, and the nature and extension of the process zone near the crack tip. An accurate three-dimensional finite-element analysis of the *DT* specimen was performed and the detailed methodology is described therein. Evans' method was shown to underestimate the stress-corrosion index by an amount up to 30%, even operating inside the range in which  $K_I$  is constant within 5%. This note reports the application of such a methodology to lava rocks.

\*Corresponding author. Tel.: +390-51-2095016; fax: +390-51-2095058.

E-mail address: matteo@ibogeo.df.unibo.it (M. Ciccotti).

### 2. Test materials

The lava rock specimens are from Vulcano, Aeolian Islands, Italy. Specimen V2 was taken from the Fossa latitic eruption, V3 comes from the Lentia rhyolitic dome. On the first specimen we could perform two consecutive relaxations ( $r_1$  and  $r_2$ ). A specimen of quartz-feldspar sandstones (C3) from the locality of Castrola, Castel di Casio, Italy was also tested. The two lava specimens were analyzed for their importance in representing the typical eruptive products of Vulcano island, which is the site of one of the major explosive volcanoes of the Mediterranean basin, while the Apennine sandstone is a very common construction material in the whole of Italy. The geometric parameters of the specimens are reported in Table 1.

### 3. Application of the corrective method

For each model geometry, the finite-element analysis produced a set of five corrective coefficients  $\xi$  for the compliance and five coefficients  $\psi$  for its derivative, relative to different crack lengths (tables may be found in [5, 6]). To obtain the adequate corrective functions, the set of coefficients for the geometry of the specific specimen used in the test should first be determined, and then the coefficients should be interpolated to provide for a smooth function.

#### 3.1. Aspect ratio

Corrective coefficients are assumed to be the same for specimens with identical aspect ratio  $d:W:L$ . The first operation to perform is therefore to scale the model geometries to the specimen size. The most suitable solution would be to produce specimens with the same aspect ratio as the ones analyzed in the finite-element study. However, if one needs to correct preexisting data,

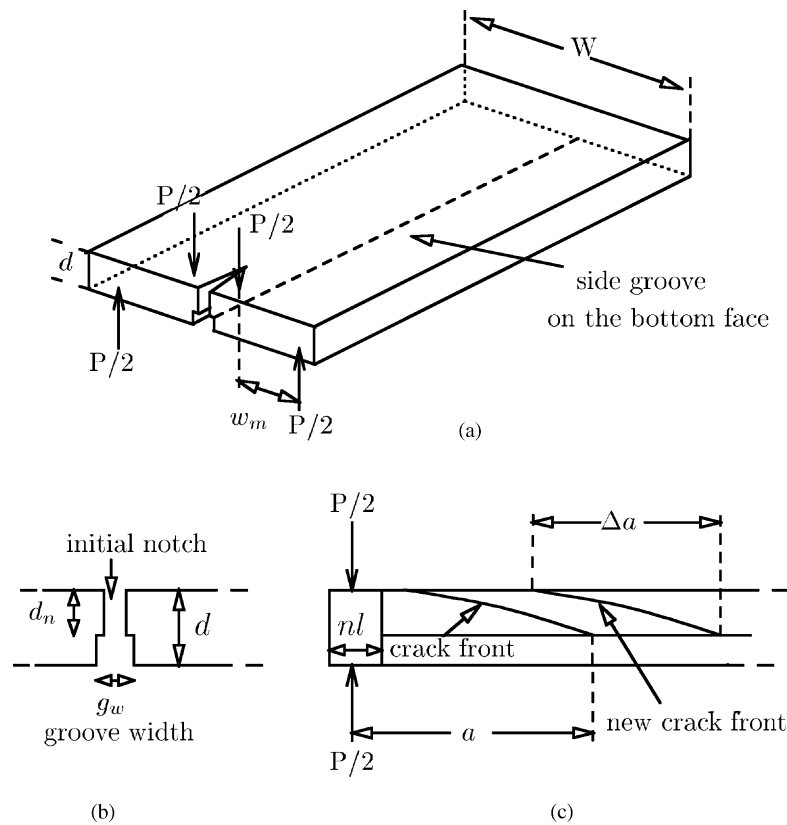


Fig. 1. Sketch of a double torsion specimen: (a) general view, (b) axial cross-section, (c) longitudinal cross-section.  $d$ ,  $W$ ,  $L$  are the thickness, width and length of the specimen,  $d_n$  is the thickness along the groove,  $g_w$  the width of the groove,  $n_l$  the length of the notch,  $P$  the applied load,  $w_m$  the moment arm of the couple,  $a$  the crack length (modified after Atkinson [2]).

Table 1  
Geometrical properties of the rock specimens V2, V3 and C3, along with the properties of the corresponding scaled models (SM)<sup>a</sup>

Specimen	$d$	$W$	$L$	$d : W : L$	$d_n/d$	$g_w$	$n_l$	$a_0$
V2	8.4	69.5	190	1 : 8.3 : 22.8	2/3	1.8	10	10
SM-V2	8.1	69.5	197	1 : 8.6 : 24.3	2/3	0; 2.32	0; 23.2	5.8
V3	6.0	81.4	212	1 : 13.7 : 35.6	4/5	1.8	11	11
SM-V3	5.9	84.0	210	1 : 14.3 : 35.7	2/3; 1	1.68; 3.36	0; 16.8	4.2
C3	5.3	71.1	161	1 : 14.0 : 30.4	5/7	2.0	10	5
SM-C3a	5.2	73.5	125	1 : 14.3 : 24.3	2/3; 1	1.67; 2.94	0; 14.7	3.7
SM-C3b	5.2	73.5	184	1 : 14.3 : 35.7	2/3; 1	1.67; 2.94	0; 14.7	3.7

<sup>a</sup>Two values of the model properties are reported when interpolation is necessary. Two different scaled models were used for specimen C3 since the actual length is intermediate between the two. All lengths are measured in mm.  $d$  is the thickness,  $W$  the width,  $L$  the length,  $d_n$  the thickness along the groove,  $g_w$  the groove width,  $n_l$  the length of the notch,  $a_0$  the distance of the loading points from the end of the specimen.

as in many practical cases, interpolation between different aspect ratios may be attempted.

The aspect ratios of specimens V2 and V3 (see Table 1) are very similar to the model geometries with  $d = 7$  mm,  $W = 60$  mm,  $L = 170$  mm and  $d = 7$  mm,  $W = 100$  mm,  $L = 250$  mm, respectively. The scaling ratios to be applied to such models are, respectively  $(1.16 \pm 0.04)$  and  $(0.84 \pm 0.02)$ . Specimen C3

has the same  $d : W$  ratio as the model specimens with  $d = 7$  mm and  $W = 100$  mm, but an intermediate length between  $L = 170$  and  $250$  mm. Two series of coefficients have been calculated for the two lengths with the same scaling ratio  $(0.735 \pm 0.006)$ , then a further interpolation between different lengths has been performed.

Once the appropriately scaled model is derived, linear interpolation of the effect of all other parameters can be

performed in cascade. In other words, one should consider the sets of five coefficients corresponding to all combinations of interesting parameters (see Table 1) and perform linear combinations between all couples of sets only differing for that parameter. One should then consider the next parameter and repeat the same operation on the resulting reduced set, and so on until one obtains a single set of coefficients relative to the specimen. The suggested interpolation order is to start from the notch length, then the groove width and finally the groove depth.

### 3.2. Effective notch length

Provided that the notch extends towards the center of the specimen past the loading points, the external part of the specimen does not affect the strain energy. As a consequence, the part of the notch that should be compared among different specimens is the one exceeding the position of the loading points. For example, for specimen V2, the effective notch length is 0 mm and the effective values for the scaled model are  $-5.8$  and  $17.4$  mm. One should not be surprised about negative notch length; this simply accounts for the compressional effect of the part standing before the loading points—resulting in a reduced compliance.

### 3.3. Crack front inclination

Since typical front inclination is  $c = \Delta a/d_n = 5$  [1], the maximum crack front inclination explored,  $c = 4$ , should be used. Higher values of  $c$  could not be modeled due to the limitations in the skewness of the elements that are required to perform an accurate numerical analysis.

### 3.4. Interpolation of the corrective functions

Once the two sets of five coefficients  $\xi$  and  $\psi$  along with the relative crack lengths for the scaled model have been obtained, smooth functions should be interpolated to provide solutions for all crack lengths inside the explored domain. An appropriate choice for smoothing the corrective factors  $\psi(a)$  appears to be a least-squares third-degree polynomial fit. The corrective coefficients  $\xi$  are best approximated by fitting the normalized compliance  $\xi(a)$ ,  $a$  with a second-order polynomial fit and then dividing by the crack length.

The interpolating functions for specimens V2 and V3 are as follows:

$$\psi_{V2}(a) = 7.224 \times 10^{-4} a^3 - 2.013 \times 10^{-2} a^2 + 1.866 \times 10^{-1} a + 3.898 \times 10^{-1}, \quad (2)$$

$$\xi_{V2}(a) = 3.554 \times 10^{-3} a + 9.032 \times 10^{-1} + 8.385 \times 10^{-1} \frac{1}{a}, \quad (3)$$

$$\psi_{V3}(a) = 8.296 \times 10^{-4} a^3 - 2.404 \times 10^{-2} a^2 + 2.268 \times 10^{-1} a + 2.223 \times 10^{-1}, \quad (4)$$

$$\xi_{V3}(a) = 7.401 \times 10^{-3} a + 8.221 \times 10^{-1} - 4.323 \times 10^{-2} \frac{1}{a}. \quad (5)$$

Concerning specimen C3, the curves for both values of the length of the scaled models should be interpolated, then a linear combination of these polynomials should be performed to obtain the curves for the actual value of specimen length

$$\psi_{C3}(a) = 2.262 \times 10^{-3} a^3 - 6.248 \times 10^{-2} a^2 + 5.837 \times 10^{-1} a - 0.941 \times 10^{-1}, \quad (6)$$

$$\xi_{C3}(a) = 1.378 \times 10^{-2} a + 6.927 \times 10^{-1} - 3.908 \times 10^{-1} \frac{1}{a}. \quad (7)$$

The values of the coefficients  $\xi$  and  $\psi$  for the three specimens are reported in Table 2 and plotted in Figs. 2–5 along with the corresponding interpolating curves.

The approximation errors for both  $\psi$  and  $\xi$  do not exceed 0.7% indicating that polynomials provide a good interpolation within the ranges of the coefficients. We do not recommend any extrapolation out of such ranges.

### 3.5. Analysis of relaxation data

The load relaxation data were pretreated to remove the external relaxation of the loading machine and the oscillations due to the cycles of thermoregulation. This produced smooth interpolation curves (splines) for  $P(t)$  and for the derivative  $dP/dt$ .

The corrective method described in [6] is then applied to obtain the  $K_I - v$  curves which are reported in Fig. 6 along with the corresponding curves resulting from Evans' model. Measures of the final load and crack length were generally used as a reference point due to their higher stability.

As we can see, the changes affect both the placement and the slope of the curves. The values of the stress corrosion index reported in Table 3 were obtained by linear fit. As expected, the values of  $n$  are generally larger than the ones obtained by Evans' analysis by an amount up to 19%.

### 3.6. Improved coefficient $\phi$

Virkar and Gordon [7] showed that the crack velocity and  $K_I$  are not constant along the front due to its

Table 2

Corrective factors  $\zeta$  and  $\psi$  along with the five corresponding values of the crack length  $a$ , as obtained by the interpolation process for specimens V2, V3 and C3 (see Table 1 for their geometric properties)<sup>a</sup>

SM-V2					
a	5.2 cm	7.5 cm	9.8 cm	12.1 cm	14.5 cm
$\zeta$	1.082	1.042	1.024	1.014	1.013
$\psi$	0.918	0.961	0.968	0.980	1.068
SM-V3					
a	4.6 cm	7.1 cm	10.5 cm	13.8 cm	17.2 cm
$\zeta$	0.844	0.870	0.899	0.917	0.948
$\psi$	0.840	0.911	0.922	0.949	1.224
SM-C3a					
a	5.7 cm	8.2 cm	10.8 cm	13.3 cm	15.8 cm
$\zeta$	0.692	0.719	0.766	0.805	0.850
$\psi$	0.541	0.872	0.892	0.954	1.147
SM-C3b					
a	4.7 cm	7.3 cm	10.8 cm	14.2 cm	17.6 cm
$\zeta$	0.691	0.765	0.823	0.860	0.896
$\psi$	0.763	0.880	0.900	0.928	1.136

<sup>a</sup>The values of the crack length are measured starting from the loading points.

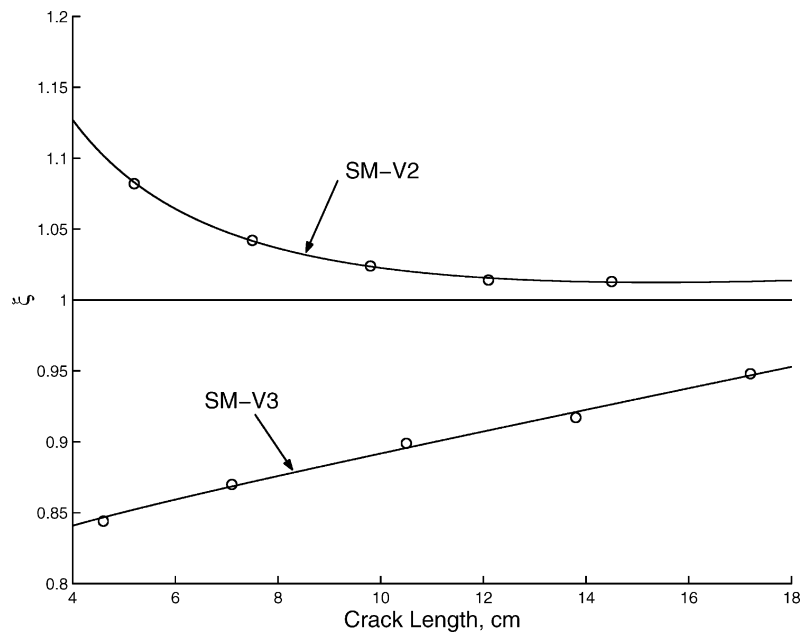


Fig. 2.  $\zeta$  coefficients and interpolated curves for the two scaled models (SM) related to specimens V2 and V3 (see Table 2).

curvature. Pollet and Burns [8] showed that averaging may be accomplished by simply changing the expression of coefficient  $\phi$  in Evans' equations

$$\phi = \left[ \frac{1}{d_n} \int_0^{d_n} \sin \alpha(x)^{1/n} dx \right]^n, \quad (8)$$

where  $\alpha$  is the inclination of the fracture front relative to the specimen surface as a function of depth  $x$  along the thickness, and  $n$  is the stress-corrosion index. If the crack front is a straight line,  $\phi$  assumes the value

proposed by Evans,  $d_n / \sqrt{\Delta a^2 + d_n^2}$ , which is just a first order correction.

Since one does not have direct measures of the crack front shape in rock specimens, following the observation that  $\Delta a / d_n$  is generally near 5 [1] it is assumed that  $\phi = 0.196$  using Evans' expression. To investigate the magnitude of the corrections we have considered some front profiles with the functional shape

$$\frac{y}{d_n} = \frac{\Delta a}{d_n} \left( \frac{x}{d_n} \right)^p, \quad (9)$$

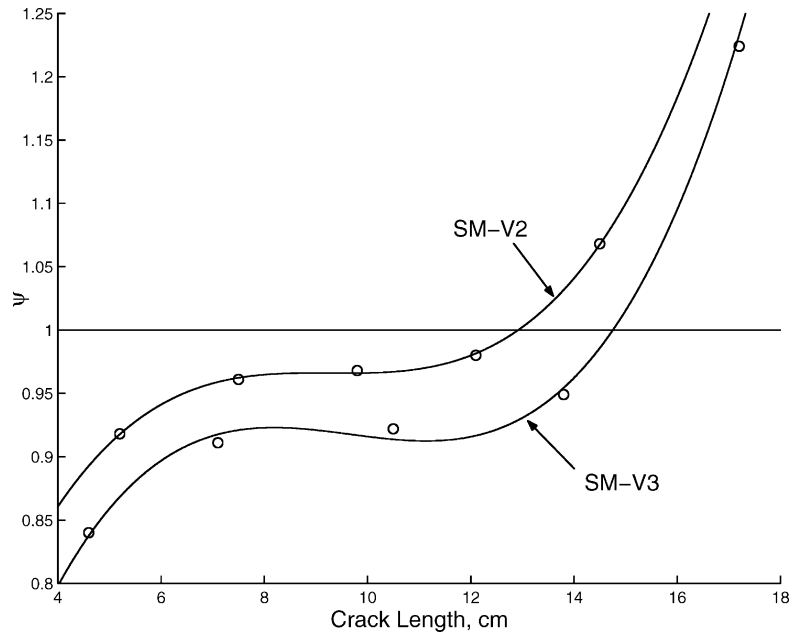


Fig. 3. Same as in Fig 2, but for  $\psi$  coefficients.

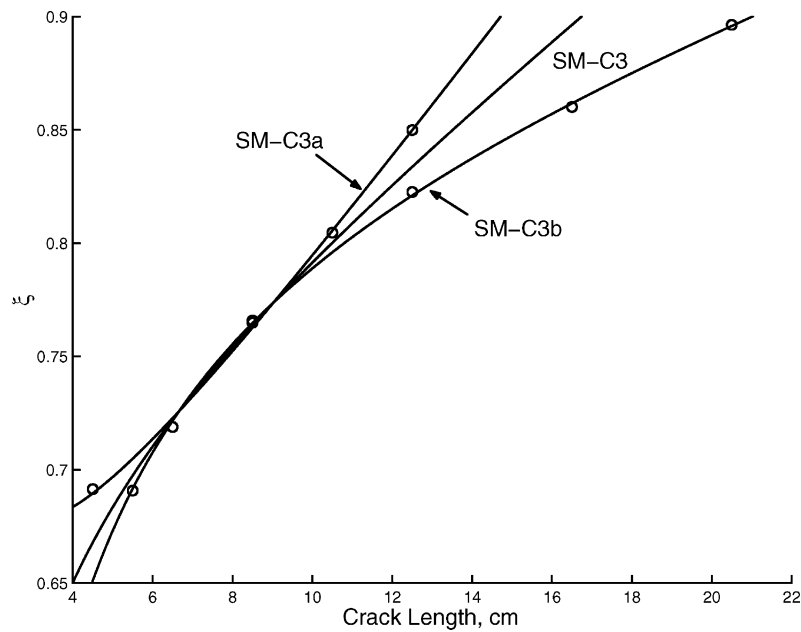


Fig. 4.  $\xi$  coefficients and interpolated curves for the two scaled models (SM) related to specimen C3 (see Table 2) along with the curve interpolated for the actual specimen length.

where  $x$  and  $y$  are as in Fig. 7, the ratio  $\Delta a/d_n$  is assumed to equal 5, and the exponent  $p$  was taken between 1 (straight line) and 4 (very curved profile). On such curves we calculated the values of  $\phi$  using Eq. (8) for values of  $n$  between 1 and 100 and verified that they are quite constant for  $n > 10$ , which is the case for most types of rocks. In Fig. 8 we reported the asymptotic

values of  $\phi$  as a function of the curvature exponent  $p$ . The parameter  $\phi$  takes Evans' value for a flat crack front ( $p = 1$ ) and increases with  $p$  eventually reaching rather large figures.

At any rate, the commonly accepted crack front profiles [9–11] are generally found to lie between curves with exponent  $p$  between 1.4 and 3.6, which correspond

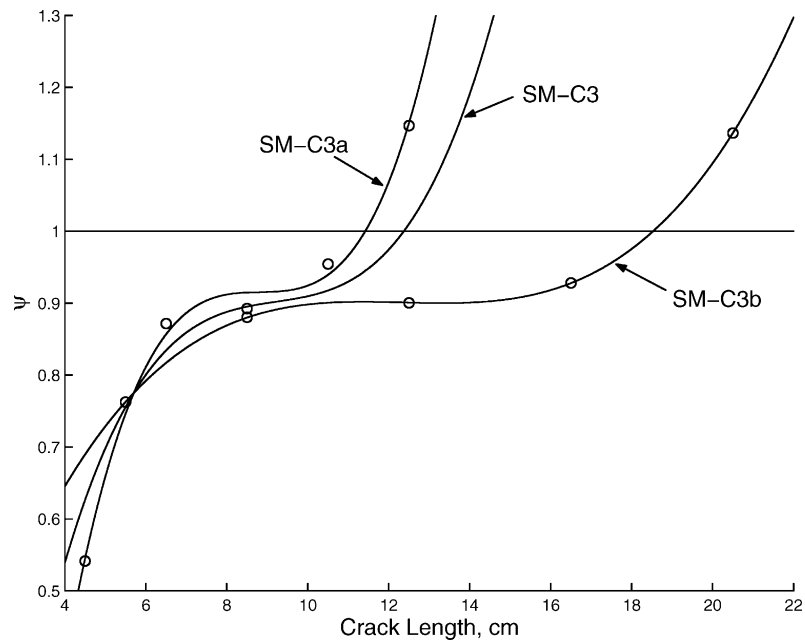


Fig. 5. Same as in Fig. 4, but for  $\psi$  coefficients.

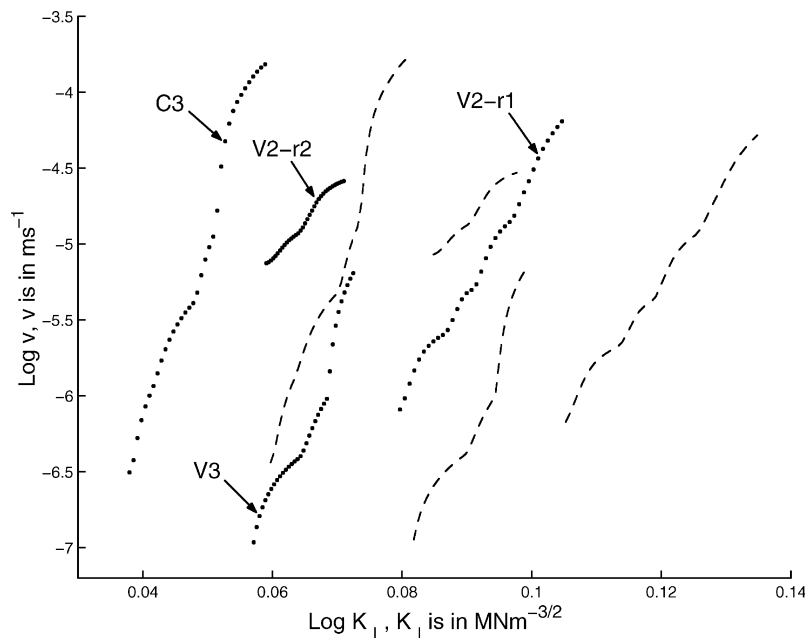


Fig. 6. Subcritical crack growth curves ( $K_I-v$ ) for the four relaxation tests. Dotted curves were obtained with the new corrected equations. Dashed curves shifted on the right were obtained by the classical analytical approximation. See Table 3 for details about the linear fit.

to values of  $\phi$  between 0.2 and 0.3. For this reason we take  $\phi = 0.25 \pm 0.05$ .

Virkar and Gordon showed that the crack shape, and consequently  $\phi$ , depend on the exponent  $n$  and can then vary along a relaxation test if the  $K_I-v$  curve is not loglinear. However, if one limits the analysis to region III of subcritical crack growth (see [3] for a description

of region III),  $\phi$  will be constant. As a result, the slope remains unaltered and the logarithmic  $K_I-v$  curve is simply shifted in the  $\log v$  direction about  $\log \phi$ . The indetermination of  $\phi$  in our analysis produces uncertainties of 0.2 in the vertical shift of the curve without affecting the determinations of the stress-corrosion index  $n$ .

Table 3  
The results of our relaxation tests<sup>a</sup>

Relaxation	$\nu$	$a_i$	$a_f$	$\text{Log}A^E$	$n^E$	$\text{Log} A$	$n$	$\Delta n/n$
V2-r1	0.13	46	55	− 12.7	62.3	− 12.0	74.0	+ 19%
V2-r2	0.13	55	93	− 9.1	47.0	− 8.2	50.9	+ 8%
V3	0.22	42	61	− 18.0	129.7	− 15.7	144.5	+ 11%
C3	0.18	49	—	− 14.2	129.9	− 11.6	134.9	+ 4%

<sup>a</sup>  $\nu$  is the Poisson ratio,  $a_i$  and  $a_f$  the measures in mm of the crack length before and after the test,  $\text{Log}A^E$  and  $n^E$  are, respectively, the constant term and the stress-corrosion index obtained with the classical Evans method,  $\text{Log} A$  and  $n$  are the values resulting from our new analysis,  $\Delta n/n$  shows the relative variation.

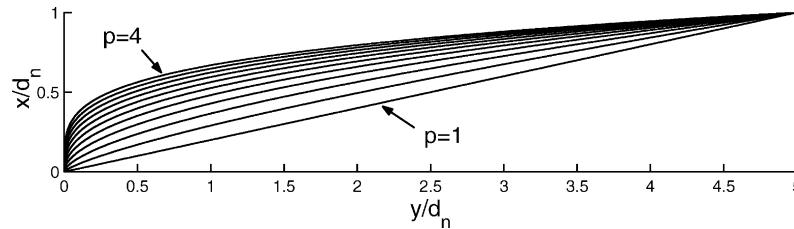


Fig. 7. Curved crack front profiles obtained through Eq. (9). The curvature exponent  $p$  ranges from 1 to 4 in 10 steps of 0.3.

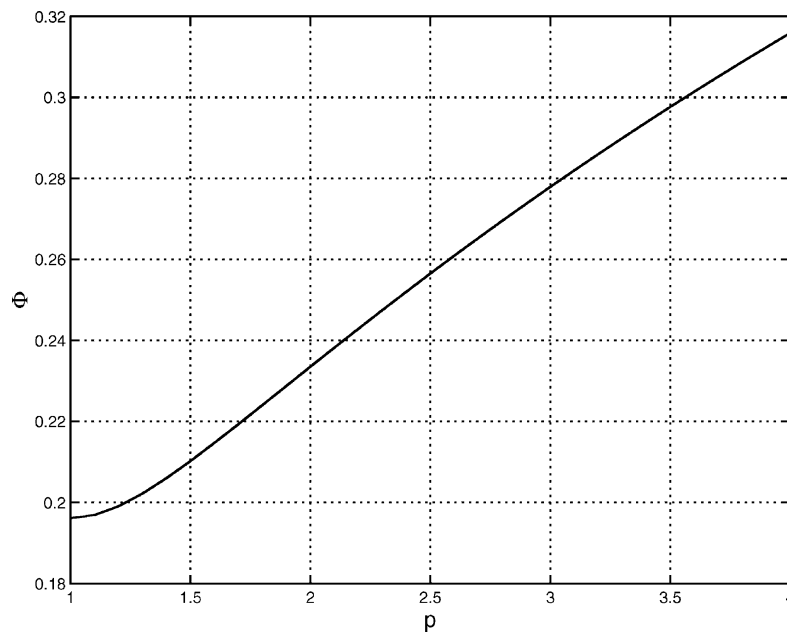


Fig. 8. Asymptotic values ( $n \gg 10$ ) of  $\phi$  as a function of the curvature exponent  $p$ .  $\phi$  assumes Evans' value for flat crack front ( $p = 0$ ) and increases with  $p$  eventually reaching rather large values.

#### 4. Conclusion

The finite-element analysis performed by Ciccotti [5] shows that Evans' analytical approximation is inadequate to describe the double torsion loading configuration except in a very narrow region of very thin specimens. The calculated corrective coefficients allow one to use a wider region of the specimen and to account

for the influence of some geometrical features like the depth and width of the side groove, the length of the initial notch and the inclination of the curved crack front.

The application of this method to relaxation tests on lava rocks from the Vulcano volcano in the Aeolian Islands, and quartz-feldspar sandstones from Castel di Casio, Italy, showed that the corrected estimates of the

stress-corrosion index are larger than the ones obtained through the classical analytical approximation by about 10%. Moreover, an estimate of the error introduced in the placement of the curves by an inaccurate knowledge of the crack front curvature was evaluated using the improved  $\phi$  factors proposed by Pollet [8].

### Acknowledgements

This work has been performed with partial contribution from GNV/INGV.

### References

- [1] Evans AG. A method for evaluating the time-dependent failure characteristics of brittle materials — and its applications to polycrystalline alumina. *J. Mater. Sci.* 1972;7:1137–46.
- [2] Atkinson BK. Technical note. *Int. J. Rock Mech. Min. Sci. Geomech. Abstr.* 1979;16:49–53.
- [3] Atkinson BK. Subcritical crack growth in geological materials. *J. Geophys. Res.* 1984;89:4077–114.
- [4] Swanson PL. Subcritical crack growth and other time- and environment- dependent behavior in crustal rocks. *J. Geophys. Res.* 1984;89 B6:4137–52.
- [5] Ciccotti M. A realistic finite-element model for the Double Torsion loading configuration. *J. Am. Ceram. Soc.* 2000;83(11): 2737–44.
- [6] Ciccotti M, Gonzato G, Mulargia F. The double torsion loading configuration for fracture propagation: an improved methodology for the load-relaxation at constant displacement. *Int. J. Rock Mech. Min. Sci.* 2000;37:1103–13.
- [7] Virkar AV, Gordon RS. Crack front profiles in double-torsion specimens. *J. Am. Ceram. Soc.* 1975;58:536–7.
- [8] Pollet JC, Burns SJ. Crack velocity correction factor for the crack-front shape in double-torsion specimens. *J. Am. Ceram. Soc.* 1979;62:426–7.
- [9] Trantina GG. Stress analysis of the double torsion specimen. *J. Am. Ceram. Soc.* 1977;60:338–41.
- [10] Pabst RF, Weick J. Double torsion measurements with and without a guiding notch. *J. Mater. Sci.* 1981;16:836–8.
- [11] Williams DP, Evans AG. A simple method for studying slow crack growth. *J. Test. Eval.* 1973;1:264–70.